Modeling water penetration at dam-foundation joint

Modeling water penetration at dam-foundation joint

Fabrizio Barpi[1], Silvio Valente[2]

[1]Dipartimento di Ingegneria Strutturale, Edile e Geotecnica, Politecnico di Torino, Corso Duca degli Abruzzi 24, 10129 Torino, Italy. E-mail: *fabrizio.barpi@polito.it*

[2]Dipartimento di Ingegneria Strutturale, Edile e Geotecnica, Politecnico di Torino, Corso Duca degli Abruzzi 24, 10129 Torino, Italy. E-mail: *silvio.valente@polito.it*

Keywords Cohesive crack, Concrete, Dam Foundation, Fracture, ICOLD, Joint, Pressure Water

Abstract *When fracture occurs in a concrete dam, the crack mouth is typically exposed to water. Very often this phenomenon occurs at the dam-foundation joint and is driven also by the fluid pressure inside the crack. Since the joint is the weakest point in the structure, this evolutionary process determines the load bearing capacity of the dam. In this paper the cracked joint is analyzed through the cohesive model proposed by Cocchetti et al. (2002), which takes into account the coupled degradation of normal and tangential strength. The water pressure inside the crack, which reduces fracture energy and increases the driving forces, is analyzed through the model proposed by Reich et al. (1994) and Brühwiler and Saouma (1995a, 1995b). Some numerical results are presented which refer to the benchmark problem proposed in 1999 by the International Commission On Large Dams. During the evolutionary process the horizontal dam crest displacement has been found to be a monotonic increasing function of the external load multiplier. As the fictitious process zone moves from the upstream to the downstream edge a transition occurs in the path of crack formation: the initial phase is dominated by the opening displacement, on the contrary afterwards the shear displacement dominates. Therefore, crack initiation does not depend on dilatancy. On the contrary the load carrying capacity depends on dilatancy.*

Black

1 Nomenclature

- $\dot{}$: time derivative
- a, b: constants
- $A_1, A_2, B_1, B_2, C_1, C_2, D_1, D_2$: coefficients of the polynomial function Φ
- c_1: cohesion corresponding to the knee point of $c_0 - w$ relationship
- $\bar{c}$: residual tangential stress
- c_0: cohesion
- χ_0: ultimate tensile strength
- χ_1: stress corresponding to w_1 of the $\chi - w$ relationship
- φ_i: i^{th} activation function
- $\mathcal{G}_F$: fracture energy
- $\mathcal{G}_F^{II}$: pure Mode II fracture energy
- $\mathcal{G}_F^{IIa}$: Mode II fracture energy
- $\mathcal{G}_F^{I}$: Mode I fracture energy
- γ_f: maximum overtopping coefficient
- h_f: imminent failure flood level
- h_c: dam crest height
- h_{n0}, h_{n1}: slopes of $\chi - w$ relationship
- h_{t0}, h_{t1}: slopes of $c - w$ relationship
- λ_i: plastic multiplier related to $\boldsymbol{V}_i$ $(i = 1 \dots 10)$
- μ: Coulomb friction angle
- μ_{d0}: parameter related to dilatant behaviour
- p_n: normal traction across the joint
- p_t: tangential traction across the joint
- p_w: water pressure
- p_{w0}: upper limit of water pressure
- S: damage number (used to scale the stress-opening law, see $\hat{w}$)
- w_{dil}: dilatancy parameter
- $\hat{w}$: scaled openings
- Ψ: ratio between w and w_{w0}

- Φ: ratio between p_w and p_{w0}
- κ: constant
- Q: plastic potential
- w_n: normal displacement of the joint
- w_t: tangential displacement of the joint
- w_{w0}: parameter used to define the pressure inside the crack
- w_{c_1}: opening corresponding to the knee point of $c - w$ relationship
- w_1: opening corresponding to the knee point of $\chi - w$ relationship
- ξ: constant
- $\boldsymbol{K_0}$: stiffness matrix of the interface
- $\boldsymbol{\lambda}$: vector of plastic multipliers
- $\boldsymbol{\chi}$: internal variables
- $\boldsymbol{\varphi}, \boldsymbol{N}, \boldsymbol{H}, \boldsymbol{\chi_0}, \boldsymbol{N_d}$: matrices of the Linear Complementarity Problem
- $\boldsymbol{p}$: traction vector across the joint
- $\boldsymbol{V}_i$: i^{th} inelastic displacement direction
- $\boldsymbol{w}$: displacement discontinuity vector
- $\boldsymbol{w}^e$: elastic displacement discontinuity vector
- $\boldsymbol{w}^p$: plastic displacement discontinuity vector

2 Introduction

When cracking occurs in a concrete dam the crack mouth is typically exposed to water. Very often this phenomenon occurs at the dam-foundation joint and is driven also by the fluid pressure inside the crack. Since the joint is the weakest point in the structure, this evolutionary process determines the load bearing capacity of the dam. In this paper the cracked joint is analyzed through the model proposed by Cocchetti et al. [1] (shortened CMS), which takes into account the coupled degradation of normal and tangential strength at the dam-foundation interface. The water pressure inside the crack, which reduces fracture energy and increases the driving forces, is analyzed through the model proposed in [2], [3] and [4]. The crack opening displacement induces two consequences:

- concrete permeability increases,
- water pressure increases.

Each one of these two phenomena drives the other. Some results are presented which refer to the benchmark problem proposed in 1999 by the International Commission On Large Dams [5]. Similar water-fracture interaction phenomena are observed in the analysis of retaining walls and rock slope stability.

3 Joint models

A joint is a locus of possible displacement discontinuities. The separation phenomenon is analyzed in the plasticity framework since an irreversible process occurs. The displacement vector $\boldsymbol{w}$ is assumed to be the sum of a reversible (superscript e) and an irreversible (superscript p) contribution:

$$\dot{\boldsymbol{w}} = \dot{\boldsymbol{w}}^e + \dot{\boldsymbol{w}}^p \tag{1}$$

$$\dot{\boldsymbol{p}} = \boldsymbol{K_0}\,\dot{\boldsymbol{w}}^e = \boldsymbol{K_0}\,(\dot{\boldsymbol{w}} - \dot{\boldsymbol{w}}^p) \tag{2}$$

where $\boldsymbol{p}$ represents the traction vector across the joint and $\boldsymbol{K_0}$ the stiffness of the joint.

3.1 Damage initiation phase

According to the CMS model proposed by Cocchetti et al. [1] and Bolzon and Cocchetti [6], damage initiation occurs when the stress path achieves the piecewise linear *yield* or *activation function* shown in Fig. 1, where p_n is the normal traction, χ_0 its ultimate value in pure tension, p_t is the tangential traction, c_0 the cohesion and μ the Coulomb friction angle. The activation function consists of a vector of φ_i whose components or modes correspond to half-planes in the bi-dimensional stress space. The intersection of such half planes is a convex domain that constitutes the region of elastic behaviour of the joint.

Each component φ_i depends on cohesive tractions $\boldsymbol{p}$ and static internal variables $\boldsymbol{\chi}$:

$$\varphi_i = \varphi_i(\boldsymbol{p}, \boldsymbol{\chi}) \begin{cases} < 0 & \text{inactive joint} \\ = 0 & \text{active joint} \end{cases}$$

The point where damage initiation occurs is called fictitious crack tip (FCT). During the evolutionary process, it moves from the upstream edge to the downstream edge.

3.2 Damage evolution phase

Once the necessary activation condition $\varphi = 0$ is met, irreversible displacements $\dot{\boldsymbol{w}}^p$ can develop along the interface:

$$\dot{\boldsymbol{w}}^p = \frac{\partial Q(\boldsymbol{p}, \boldsymbol{\chi})}{\partial \boldsymbol{p}}\,\dot{\boldsymbol{\lambda}} \qquad \dot{\boldsymbol{\lambda}} \geq \boldsymbol{0} \tag{3}$$

where the *plastic potential* $Q(\boldsymbol{p}, \boldsymbol{\chi})$ is defined in such a way that the interface fracture work without friction is controlled as explained later. The portion of joint where damage evolves is called fictitious process zone (shortened FiPZ).

The main features that differentiates the CMS model from Carol et al. [7] and Červenka et al. [8] is that all equations are linearized, hence the nonlinearity of the model is contained only in the complementarity conditions. A first set of five relations, also referred to as *Kuhn-Tucker conditions*, can be written with reference to the plastic multiplier $\dot{\lambda}_i$ associated with the inelastic displacement direction $\boldsymbol{V}_i$ (shown in Fig. 1). Following Puntel [9], we can write:

$$\varphi_i \leq 0 \quad \dot{\lambda}_i \geq 0 \quad \varphi_i\,\dot{\lambda}_i = 0 \tag{4}$$

When the stress path is inside the elastic domain, all components φ_i are negative and therefore all components $\dot{\lambda}_i$ vanish. When the stress path achieves the activation function, a component φ_i vanishes and the corresponding $\dot{\lambda}_i$ becomes positive. A first set of complementarity relations specifies the conditions for the onset of softening along a branch.

Now a second set of complementarity relations has to be introduced. When the traction mode ($\varphi_1 = 0$) is activated, the linear softening law is completely determined by the condition

that the energy dissipated is the traditional Mode I fracture energy $\mathcal{G}_F^I$ [10]. The softening branch is bounded; when the displacement discontinuity, along a pure traction mode, reaches the values w_1 and w_c, the complementarity relations sixth and seventh applies.

Similarly, when two shear modes ($\varphi_4 = 0$) or ($\varphi_5 = 0$) are activated, the linear softening law is completely determined by the condition that the energy dissipated is the Mode II fracture energy $\mathcal{G}_F^{IIa}$ under high normal confinement and no dilatancy proposed in [11] in the context of the microplane model. The determination of pure Mode II fracture energy $\mathcal{G}_F^{II}$ would require a pure shear test, without normal confinement, which is extremely difficult to perform. That is the reason why $\mathcal{G}_F^{IIa}$ is preferred as a material property. The softening branch is bounded; when interface fracture work without contribution from friction, along a pure shear mode, reaches the critical value $\mathcal{G}_F^{IIa}$, the cohesive tractions vanish and the interaction forces are due to friction alone. The condition for the arrest of softening in this case can be written through a seventh complementarity relation. When the cohesive-frictional modes ($\varphi_2 = 0$ or $\varphi_3 = 0$) are activated, the critical condition is related to both displacement discontinuity components as shown in [1]. Along this separation mode, when the condition for the arrest of softening is reached, the residual tangential stress is assumed as constant (see term $\bar{c}$ in Fig. 1).

The last complementarity relation of the model regards the dilatant behaviour associated with λ_2 and λ_3 (see μ_{d0} in Fig. 1). It appears reasonable to assume that there is a limit to the dilatancy of a joint. Therefore, plastic multiplier λ_{10} is activated in order to store the total of λ_2 and λ_3 exceeding the parameter w_{dil}. Along this separation mode, when the condition for the arrest of softening is reached, the residual tangential stress is assumed to be dependent on Coulombian friction (see the dashed line, i.e., $\mu\, p_n$, of Fig. 1).

It should be remarked that the model takes into account a bilinear relationship between tensile strength and crack opening and between cohesion and crack opening. The coordinates of knee point are (χ_1, w_1) while the slopes of the branches are h_{n0} and h_{n1} for the former and (c_1, w_{c_1}) and h_{t0} and h_{t1} for the latter, as shown in Figs 2 and 3.

Following [1] and [9], the linear complementarity problem becomes (posing $\boldsymbol{\lambda} = \{\lambda_1, \lambda_2 \dots \lambda_{10}\}^T$):

$$\boldsymbol{\varphi} = -\boldsymbol{\chi_0} + \boldsymbol{N}^T\boldsymbol{p} - \boldsymbol{H}\boldsymbol{\lambda} > 0 \qquad \dot{\boldsymbol{\lambda}} \geq 0 \qquad \boldsymbol{\varphi}^T\boldsymbol{\lambda} = 0 \tag{5}$$

where:

$$\boldsymbol{\chi_0} = \{\chi_0, c_0, c_0, c_0 + \bar{c}, c_0 + \bar{c}, \chi_0 - \chi_1, c_0 - c_1\chi_1, c_1, w_{dil}\}^T \tag{6}$$

$$\boldsymbol{N} = \begin{bmatrix} 1 & \mu & \mu & 0 & 0 & 0 & 0 & 0 & 0 & 0 \\ 0 & 1 & -1 & 1 & -1 & 0 & 0 & 0 & 0 & 0 \end{bmatrix} \tag{7}$$

$$\boldsymbol{H} = \begin{bmatrix} h_{n0} & ah_{n0} & ah_{n0} & ah_{n0} & ah_{n0} & h_{n1} - h_{n0} & 0 & -h_{n1} & 0 & 0 \\ bh_{t0} & h_{t0} & h_{t0} & h_{t0} & h_{t0} & 0 & h_{t1} - h_{t0} & 0 & -h_{t1} & 0 \\ bh_{t0} & h_{t0} & h_{t0} & h_{t0} & h_{t0} & 0 & h_{t1} - h_{t0} & 0 & -h_{t1} & 0 \\ bh_{t0} & h_{t0} & h_{t0} & h_{t0} & h_{t0} & 0 & h_{t1} - h_{t0} & 0 & -h_{t1} & 0 \\ bh_{t0} & h_{t0} & h_{t0} & h_{t0} & h_{t0} & 0 & h_{t1} - h_{t0} & 0 & -h_{t1} & 0 \\ h_{n0} & ah_{n0} & ah_{n0} & ah_{n0} & ah_{n0} & -h_{n0} & 0 & 0 & 0 & 0 \\ bh_{t0} & h_{t0} & h_{t0} & h_{t0} & h_{t0} & 0 & -h_{t0} & 0 & 0 & 0 \\ 0 & 0 & 0 & 0 & 0 & h_{n1} & 0 & -h_{n1} & 0 & 0 \\ 0 & 0 & 0 & 0 & 0 & 0 & h_{t1} & 0 & -h_{t1} & 0 \\ 0 & -1 & -1 & 0 & 0 & 0 & 0 & 0 & 0 & 1 \end{bmatrix} \tag{8}$$

Constants a and b are taken to be equal to 1. Finally, the displacements can be written as:

$$\dot{\boldsymbol{w}} = \boldsymbol{K_0}^{-1}\dot{\boldsymbol{p}} + \boldsymbol{N_d}\dot{\boldsymbol{\lambda}} \tag{9}$$

with:

$$\begin{bmatrix} \dot{w}_n \\ \dot{w}_t \end{bmatrix} = \begin{bmatrix} K_{n0} & 0 \\ 0 & K_{t0} \end{bmatrix} \begin{bmatrix} \dot{p}_n \\ \dot{p}_t \end{bmatrix} + \begin{bmatrix} 1 & \mu_{d0} & \mu_{d0} & 0 & 0 & 0 & 0 & 0 & 0 & -\mu_{d0} \\ 0 & 1 & -1 & 1 & -1 & 0 & 0 & 0 & 0 & 0 \end{bmatrix} \begin{bmatrix} \dot{\lambda}_1 \\ \dot{\lambda}_2 \\ \dots \\ \dot{\lambda}_{10} \end{bmatrix} \tag{10}$$

4 Modeling water inside the cracks

4.1 Damage inside the cracks

As a consequence of additional damage occurring inside the FiPZ due to the presence of water, it is assumed that fracture energy $\mathcal{G}_F$ reduces as pressure p_{w0} increases. The apparent value of $\mathcal{G}_F$ is assumed to be expressed by the following relationship [2]:

$$\hat{\mathcal{G}}_F = \mathcal{G}_F \left[1 - 2\,\frac{p_{w0}}{\chi_0} + \left(\frac{p_{w0}}{\chi_0} \right)^2 \right] = \mathcal{G}_F\, S \tag{11}$$

The ratio $\frac{p_{w0}}{\chi_0}$ is identified as damage number. If $\frac{p_{w0}}{\chi_0} = 0$, i.e., $S = 1$, the material is considered undamaged and therefore, the softening law is derived from the traditional fracture energy measured in dry conditions. If $\frac{p_{w0}}{\chi_0} = 1$, i.e., $S = 0$, the material is considered fully damaged and fracture energy vanishes. The stress-opening law is now assumed in such a way that the openings are scaled through the factor S:

$$\hat{w} = S\, w \tag{12}$$

4.2 Pressure distribution

The pressure distribution is assumed to be described by two polynomial functions. Defining $\Psi = \frac{w}{w_{w0}}$ and $\Phi = \frac{p_w}{p_{w0}}$, we can write:

$$\Phi = f_1(\Psi) = A_1 + B_1\Psi + C_1\Psi^2 + D_1\Psi^3 \qquad \Psi \le \Psi_1 \tag{13}$$

$$\Phi = f_2(\Psi) = A_2 + B_2\Psi + C_2\Psi^2 + D_2\Psi^3 \qquad \Psi \ge \Psi_1 \tag{14}$$

These functions are plotted in a non dimensional space in Fig. 4 (f_1: dotted, f_2: dashed). The slope at $(\Psi_0, 0)$ and $(1, 1)$ is equal to zero; the slope at (Ψ_1, Φ_1) is continuous. It must be remarked that the eight constants of Eqs 13 and 14 are obtained by imposing six geometrical conditions and two mechanical conditions.

Value Ψ_0 corresponds to crack opening w below which $p_{w0} = 0$, while Ψ_1 corresponds to the knee point w_1. Value Ψ_0 is defined as:

$$\Psi_0 = \Psi_1 - \frac{2}{\kappa}\,\Psi_1 \tag{15}$$

where $\kappa \ge 2$ is a constant.

The transition point between f_1 and f_2 is defined by the coordinate Ψ_1, see Eq. 15, and Φ_1:

$$\Phi_1 = \frac{2\,\Psi_1}{2\Psi_1 + \kappa\,(1 - \Psi_1)} \tag{16}$$

The value w_{w0} shown in Fig. 2 is assumed to be:

$$w_{w0} = \hat{w}_1 + \frac{2}{\xi}\,(\hat{w}_c - \hat{w}_1) \tag{17}$$

where $\xi \ge 2$ is a constant.

5 Example of application

5.1 Numerical model

The numerical simulations are performed in the framework of the finite element code [12] by means of the so called "user subroutines".

5.2 Benchmark problem

As an example of application, the benchmark problem proposed in 1999 by the International Commission On Large Dams [5] was analyzed. The gravity dam shown in Fig. 5 was discretized through 57313 triangular elements and the foundation through 11020, as shown in Fig. 6. The joint was discretized through 1000 quadrilateral elements (0.01m thick and 0.06m wide), the boundary through 115 infinite elements. Figure 7 shows the mesh around the crack tip. Tables 1 and 2 show the assumed material properties. The stiffness properties of the joint, necessary to determine the coefficients of Eq. 8, are those of a 0.01m thick layer of concrete. With refrenece to the continuum triangular element side (0.06m), the joint thickness (0.01m) is chosen small enough to model accurately the local behaviour but large enough to avoid loss of precision.

5.3 Numerical results

The dam is analyzed under the following conditions:

- self weight application,
- reservoir filling,
- imminent failure flood.

Since the joint is the weakest part in the structure, the remaining material behaves in a linear elastic way.

In order to deal with a ratio $\frac{p_{w0}}{\chi_0}$ belonging to the range tested in [2], an appropriate value of tensile strength χ_0 is chosen (see Table 2). After the application of the self weight, the structure behaves linearly up to 87.5% of hydrostatic water pressure corresponding to the height of the dam crest ($h_c = 80$m). Above this level, starting from the upstream right angle, where the elastic stress field is singular, a fictitious process zone begins to grow along the joint. As the load proportionality factor grows from 0.875 to 1 the crack mouth opening displacement reaches the value w_{w0} and the water pressure penetrates into the crack and becomes an additional driving force for crack propagation. Nevertheless, when the water level reaches the dam crest, the crack turns out to be still stable in load control. In the last load step the water level is fictitiously raised up to the level that leads to the collapse of the dam. This level is often termed as the level of *imminent failure flood* h_f. The load-carrying capacity and the safety of the dam against failure are evaluated in terms of the maximum overtopping coefficient $\gamma_f = \frac{h_f}{h_c}$. After each load increment, the fluid pressure acting on the crack faces is updated according to the new values of displacement discontinuity. All the states reached during the evolutionary quasi-static analysis are stable in load-control.

Figures 8 and 9 show the crack opening and sliding distribution near the crack, Fig. 10 the displacement paths. Figures 11 and 12 show the related normalized (with respect to χ_0) normal and tangential stress distribution. Finally, Figs 13, 14 and 15 show the overtopping coefficient as a function of the horizontal crest displacement, crack mouth opening and sliding displacement, respectively.

6 Conclusions

The main contribution of this research is to assess the influence of water penetration inside a dam-foundation joint. For the material properties and boundary conditions analyzed the following conclusions can be drawn:

- During the evolutionary process the horizontal dam crest displacement has been found to be a monotonic increasing function of the external load multiplier.
- As the fictitious process zone moves from the upstream to the downstream edge a transition occurs in the path of crack formation: the initial phase is dominated by the opening displacement, on the contrary afterwards the shear displacement dominates.
- The crack initiation does not depends on dilatancy. On the contary the load carrying capacity depends on dilatancy.

7 Acknowledgments

The financial support provided by the Italian Department of Education, University and Scientific Research (MIUR) to the research project on *"Diagnostic analyses and safety assessment of existing concrete dams"* (grant number 2004084599_004) is gratefully acknowledged.

References

[1] G. Cocchetti, G. Maier, and X. Shen. Piecewise linear models for interfaces and mixed mode cohesive cracks. *Journal of Engineering Mechanics (ASCE)*, 3:279–298, 2002.

[2] W. Reich, E. Brühwiler, V. Slowik, and V.E. Saouma. Experimental and computational aspects of a water/fracture interaction. In E. Bourdarot, J. Mazars, and V. Saouma, editors, *Dam Fracture and Damage*, pages 123–131, The Netherlands, 1994. Balkema.

[3] E. Brühwiler and V.E. Saouma. Water fracture interaction in concrete - Part I: Fracture properties. *American Concrete Institute Journal*, 92:296–303, 1995.

[4] E. Brühwiler and V.E. Saouma. Water fracture interaction in concrete - Part II: Hydrostatic pressure in cracks. *American Concrete Institute Journal*, 92:383–390, 1995.

[5] ICOLD. Theme A2: Imminent failure flood for a concrete gravity dam. In *Fifth International Benchmark Workshop on Numerical Analysis of Dams*, Denver (CO), 1999.

[6] G. Bolzon and G. Cocchetti. Direct assessment of structural resistance against pressurized fracture. *International Journal for Numerical and Analytical Methods in Geomechanics*, 27:353–378, 2003.

[7] I. Carol, P.C. Prat, and C.M. Lopez. A normal/shear cracking model: Application to discrete crack analysis. *Journal of Engineering Mechanics (ASCE)*, 123(8):765–773, 1997.

[8] J. Červenka, J.M.C. Kishen, and V.E. Saouma. Mixed mode fracture of cementious bimaterial interfaces; part ii: Numerical simulations. *Engineering Fracture Mechanics*, 60(1):95–107, 1998.

[9] E. Puntel. *Experimental and numerical investigation of the monotonic and cyclic behaviour of concrete dam joints*. PhD thesis, Politecnico di Milano, 2004.

[10] A. Hillerborg, M. Modeer, and P.E. Petersson. Analysis of crack formation and crack growth in concrete by means of fracture mechanics and finite elements. *Cement and Concrete Research*, 6:773–782, 1976.

[11] I. Carol, Z.P. Bažant, and P.C. Prat. Microplane-type constitutive models for distributed damage and localized cracking in concrete structures. In Z.P. Bažant, editor, *Fracture Mechanics of Concrete Structures*, pages 299–304, The Netherlands, 1992. Elsevier Applied Science.

[12] ABAQUS. *ABAQUS 6.5 Analysis User's Manual*, 2005.

[13] P.E. Petersson. Crack growth and development of fracture zone in plain concrete and similar materials. Technical Report TVBM-1006 (Division of Building Materials), Lund University of Technology, Lund (Sweden), 1981.

List of Tables

List of Figures

Dam and foundation Young modulus (Pa)	Dam and foundation Poisson ratio –	χ_0 (Pa)	c_0 (Pa)	$\mathcal{G}_F^I$ (N/m)	$\mathcal{G}_F^{IIa}$ (N/m)
2.4e10	0.15	2.0e6	6.0e6	147	514

Table 1: Material properties.

χ_1 (Pa)	c_1 (Pa)	$\bar{c}$ (Pa)	μ –	μ_{d0} –	w_1 (m)	w_c (m)	w_{dil} (m)
0.66e6	2.33e6	1.0	0.577	0.1	1.5e-4	6.75e-4	2.0e-3

Table 2: Material properties (continued).

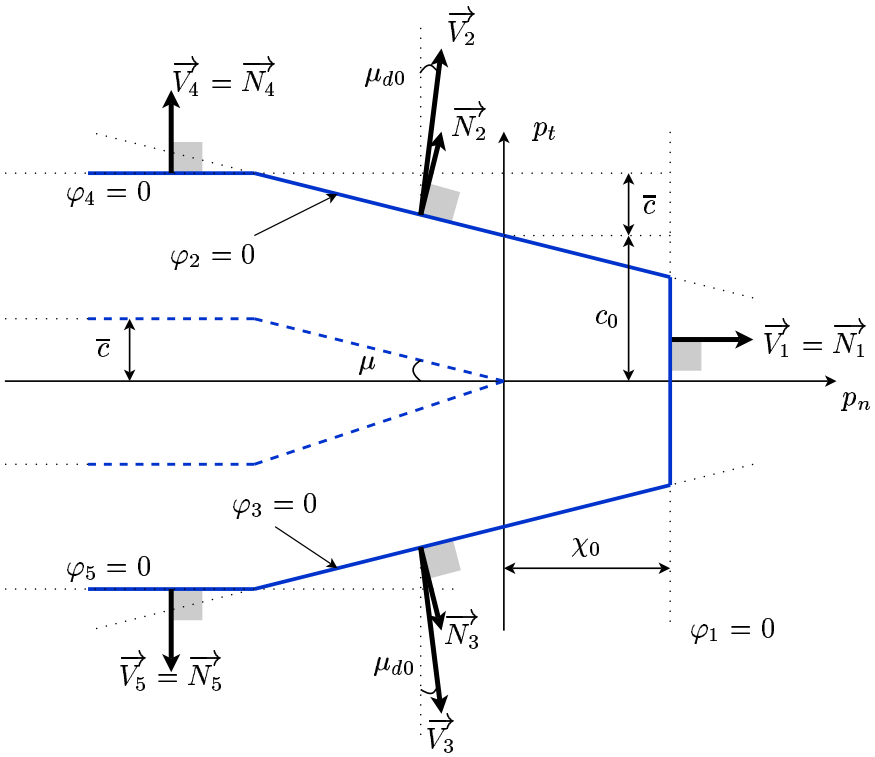

Figure 1: Piecewise linear model.

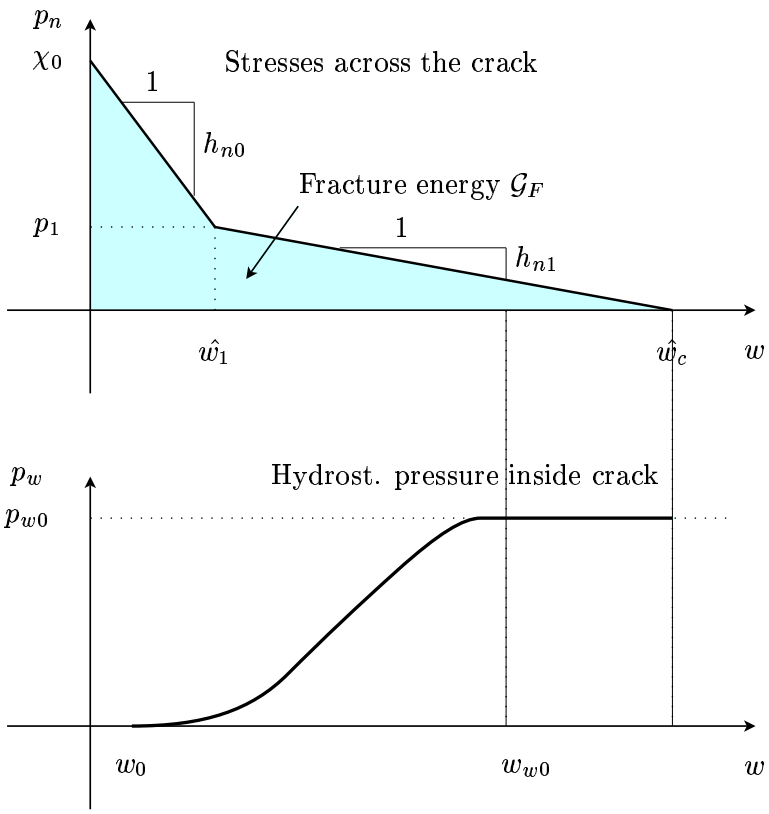

Figure 2: Water pressure distribution inside the crack. The aspect ratios of Petersson's softening law [13] are $\frac{\hat{w_1}}{\hat{w_c}} = \frac{2}{9}$ and $\frac{p_1}{\chi_0} = \frac{1}{3}$.

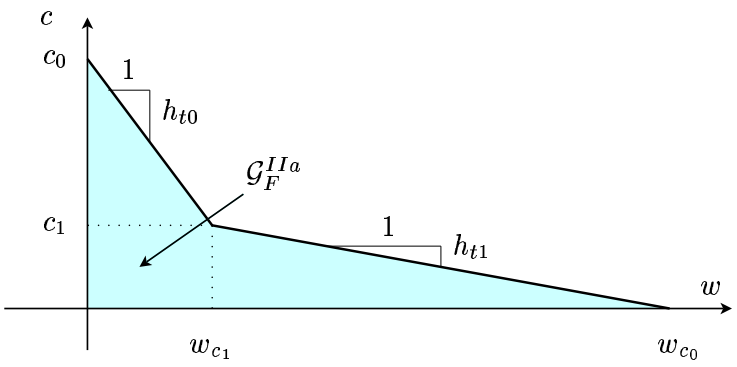

Figure 3: Softening law for cohesion. The aspect ratio is the same of Fig. 2.

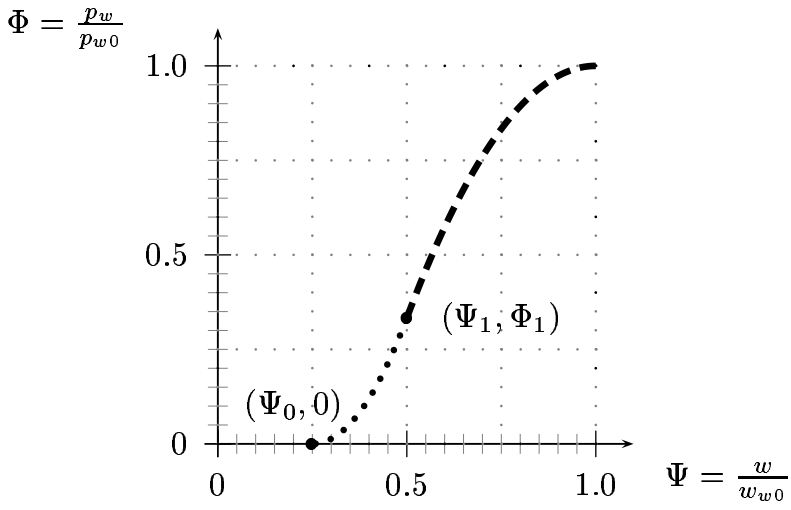

Figure 4: Hydrostatic pressure transition ($\kappa = 4, \Psi_0 = 0.25, \Psi_1 = 0.5$).

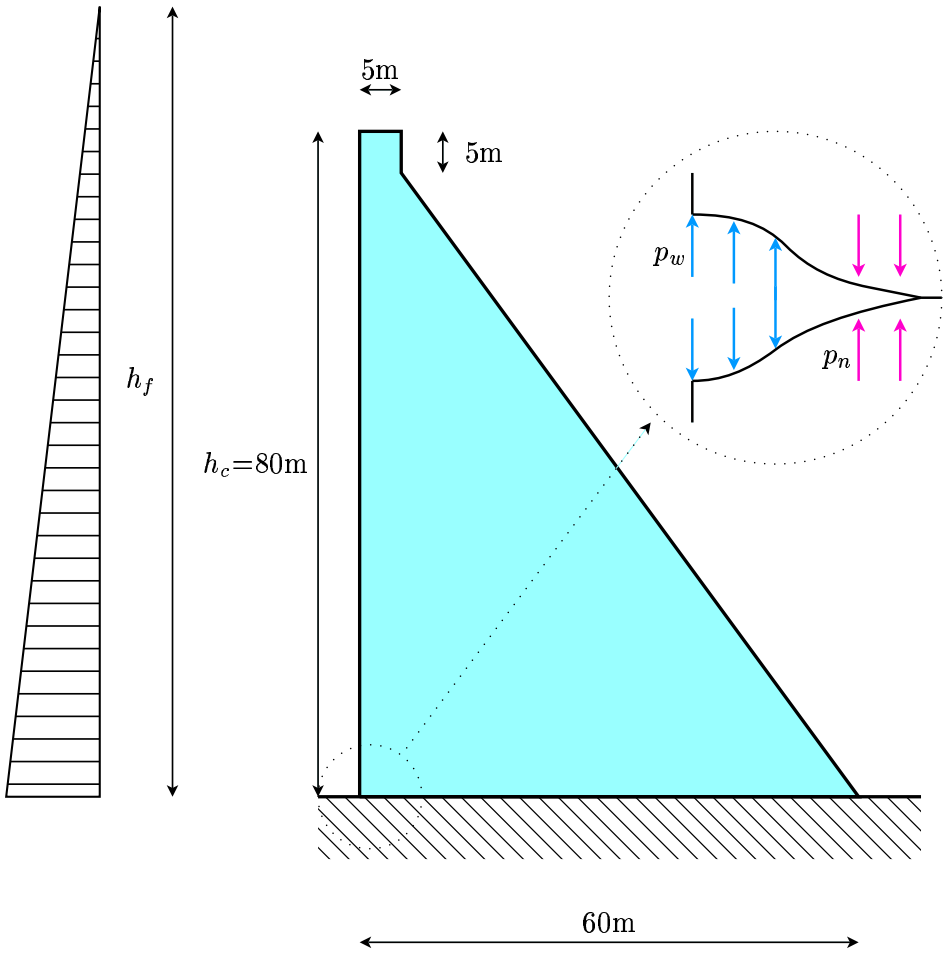

Figure 5: Gravity dam proposed as benchmark by ICOLD (1999).

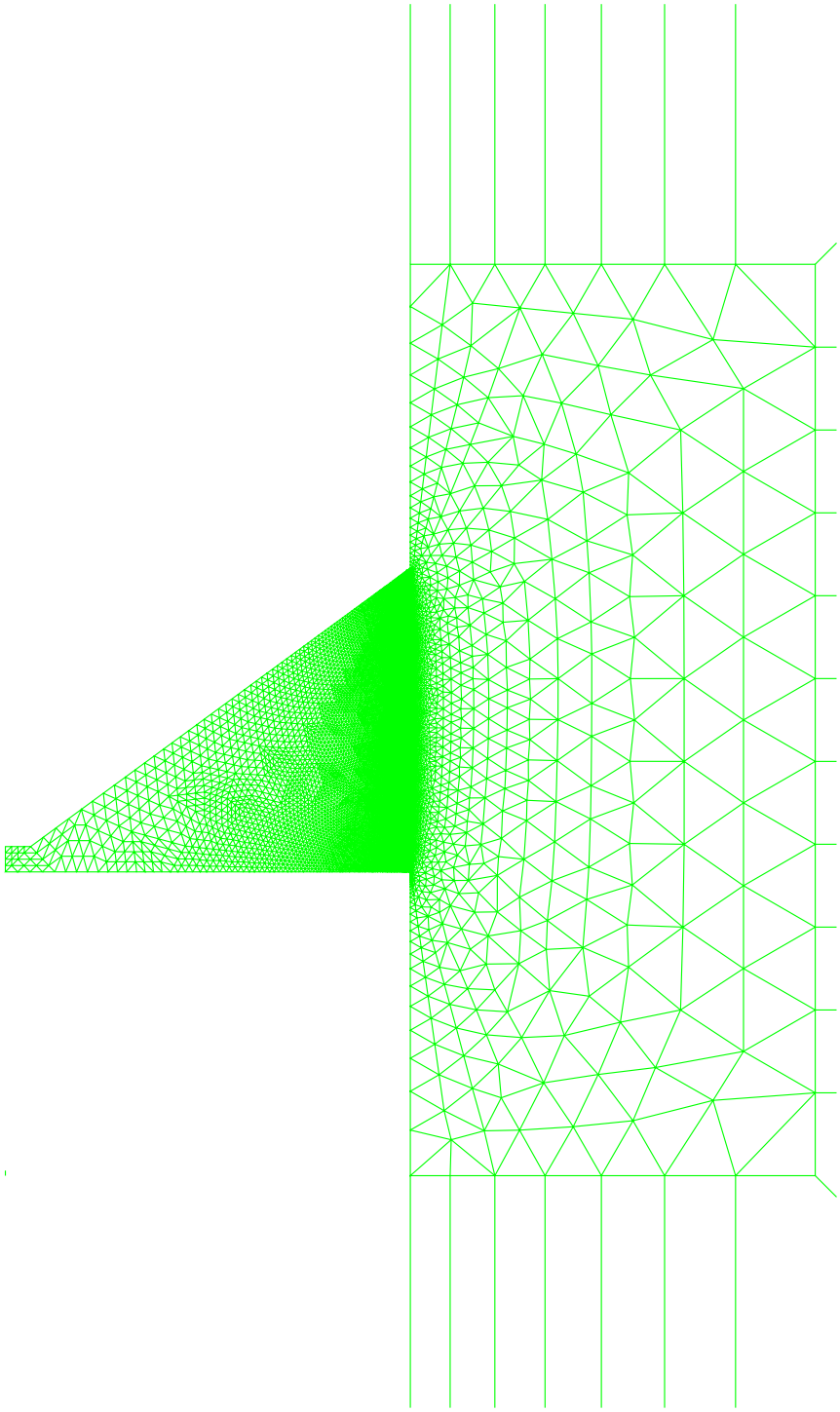

Figure 6: Mesh used in the simulations.

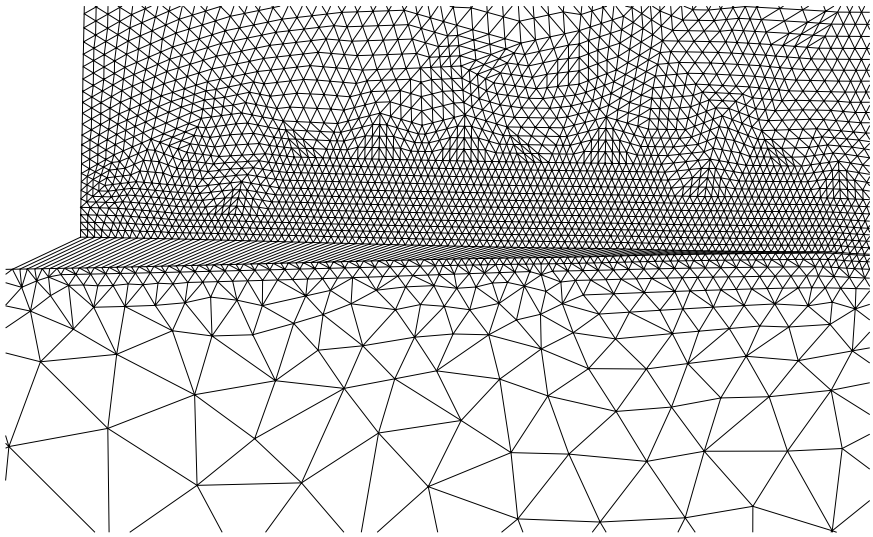

Figure 7: Mesh detail around crack tip.

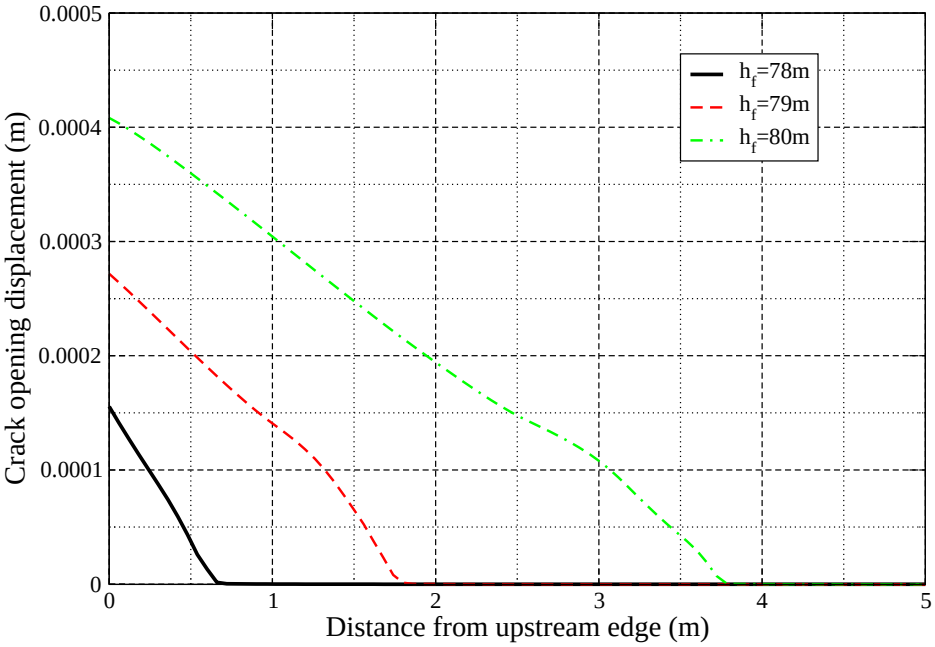

Figure 8: Crack opening displacement vs. distance from upstream edge.

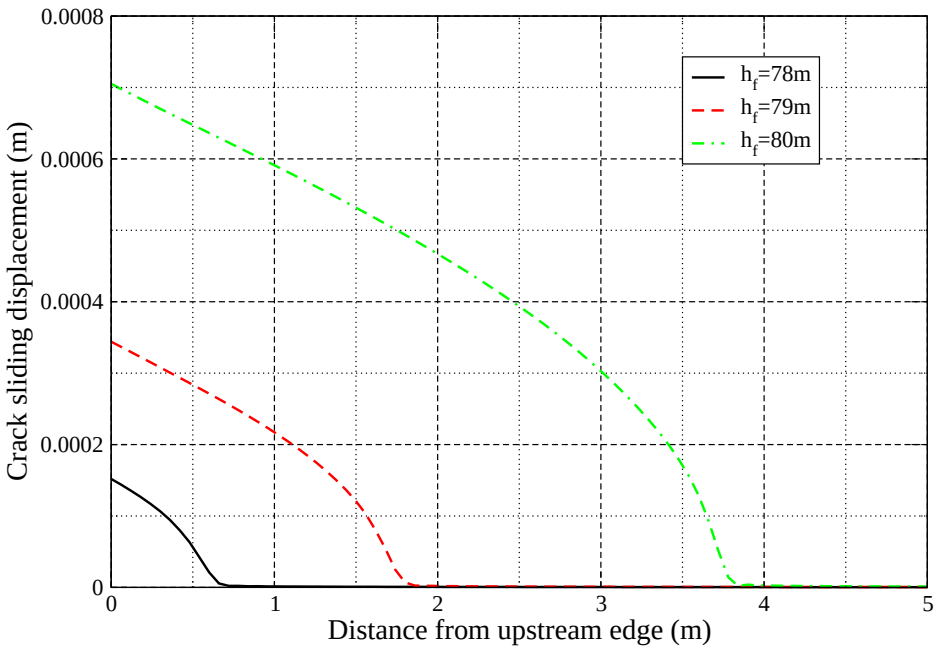

Figure 9: Crack sliding displacement vs. distance from upstream edge.

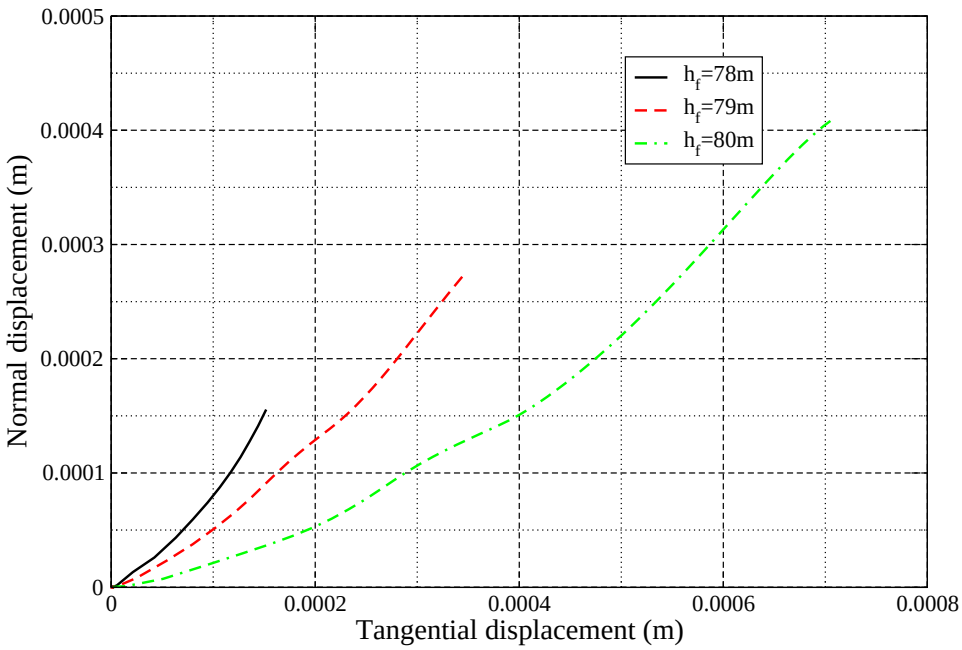

Figure 10: Displacement discontinuities for an observer moving from FCT to crack mouth.

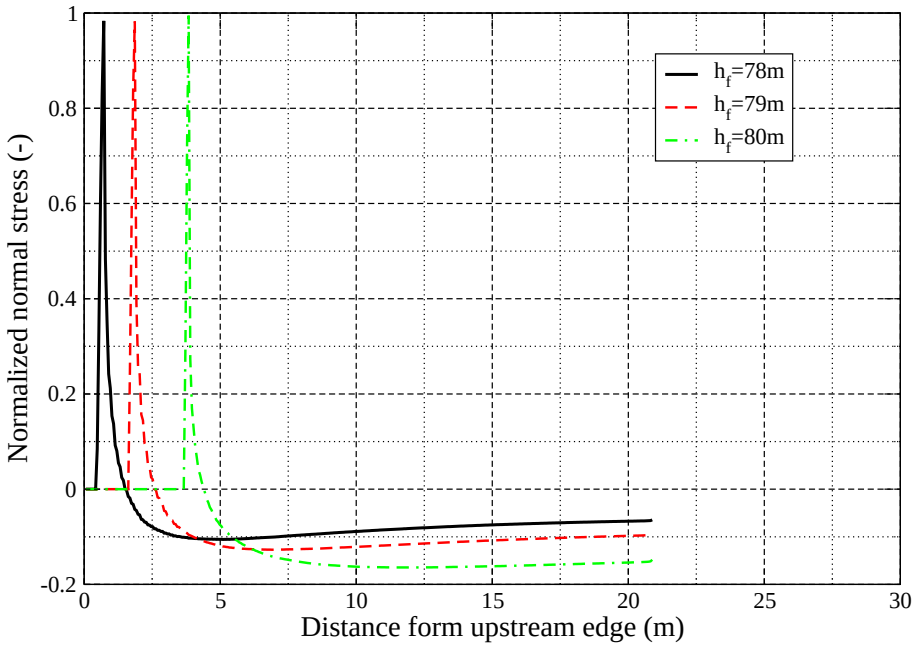

Figure 11: Normal stress vs. distance from upstream edge.

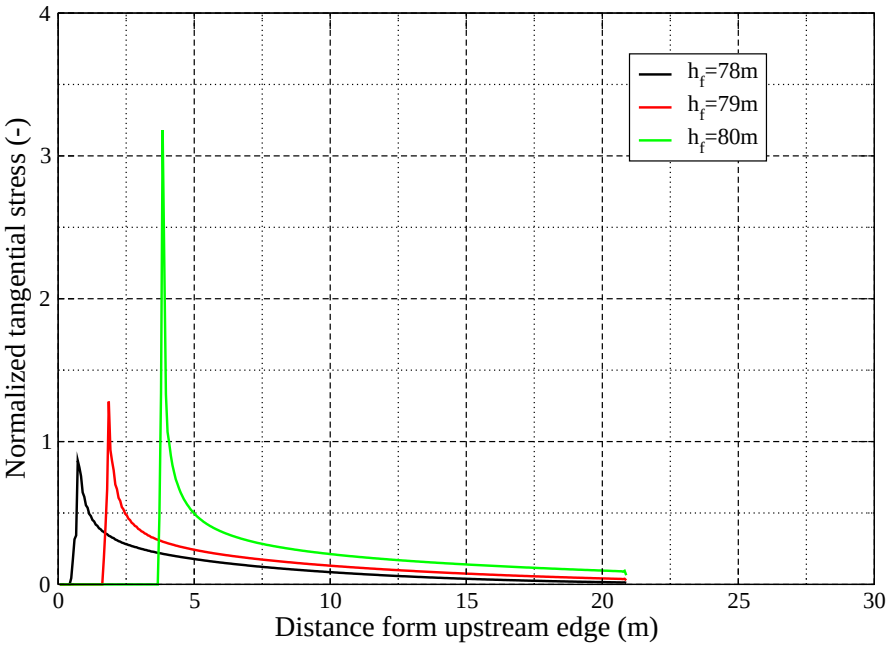

Figure 12: Tangential stress vs. distance from upstream edge.

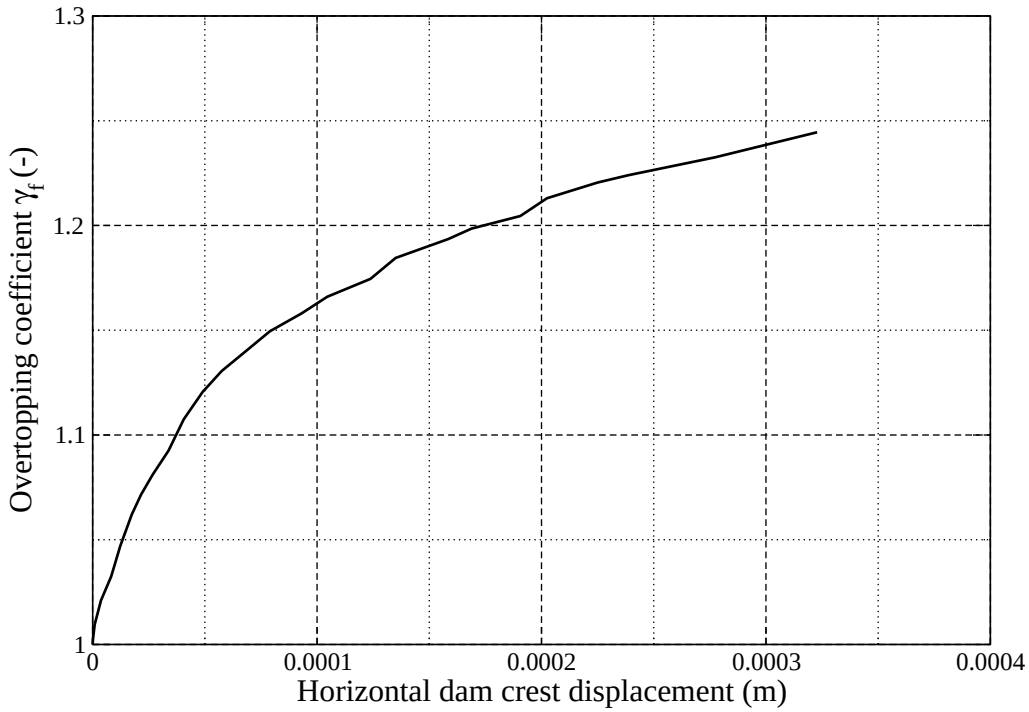

Figure 13: Overtopping coefficient γ_f vs. horizontal crest displacement (computed from time step corresponding to h_f=80m).

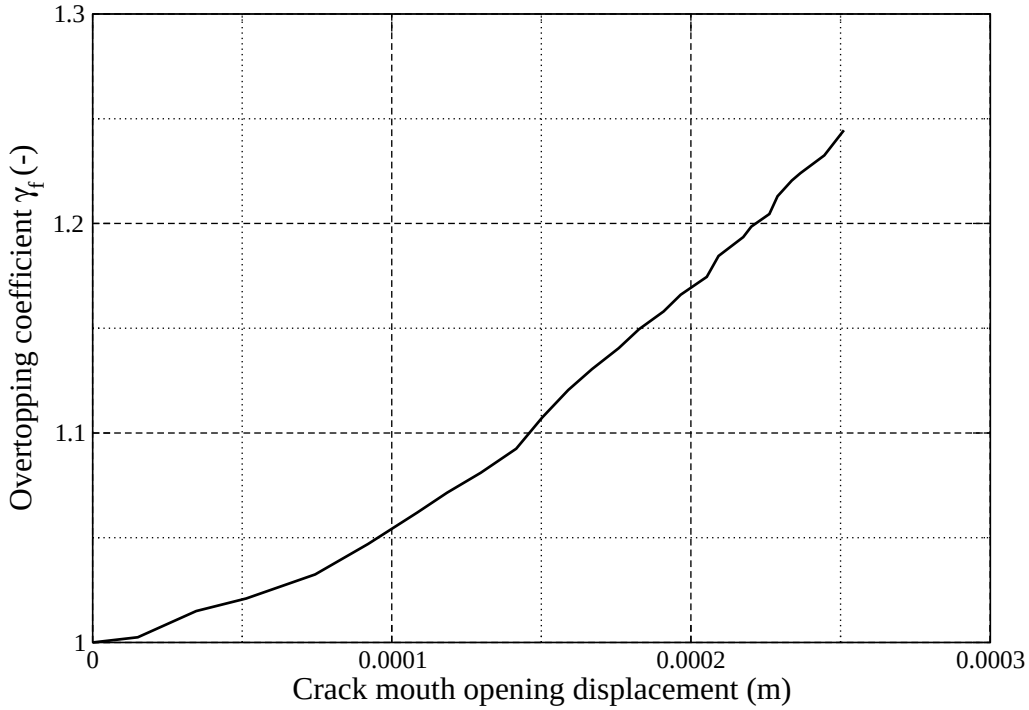

Figure 14: Overtopping coefficient γ_f vs. crack mouth opening displacement (computed from time step corresponding to h_f=80m).

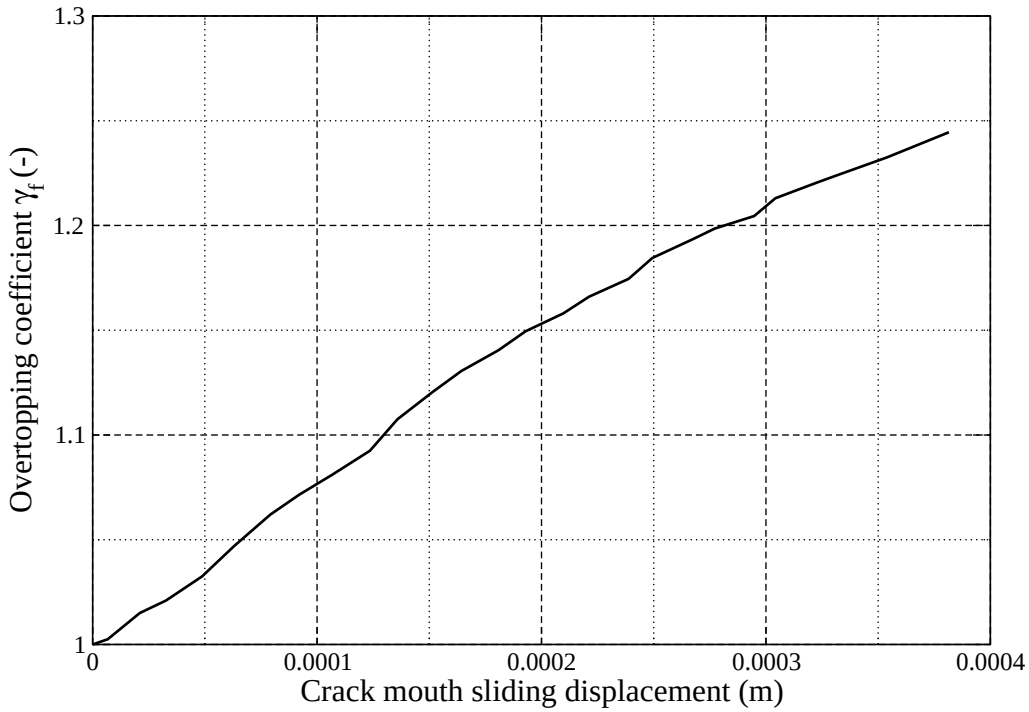

Figure 15: Overtopping coefficient γ_f vs. crack mouth sliding displacement (computed from time step corresponding to h_f=80m).